Comparison of the Dispersion Properties of Higher Order FDTD Schemes and Equivalent-Sized MRTD Schemes

Kurt L. Shlager, *Senior Member, IEEE,* and John B. Schneider

Abstract—The dispersion errors of higher order finite-difference time-domain (HO-FDTD) algorithms are compared to those of multiresolution time-domain (MRTD) algorithms that have equivalent spatial stencil sizes. Both scaling-function-based MRTD (S-MRTD) and wavelet-function-based MRTD (W-MRTD) schemes are considered. In particular, the MRTD schemes considered include the Coifman scaling functions and the Cohen–Daubechies–Feauveau (CDF) biorthogonal scaling and wavelet functions. In general, the HO-FDTD schemes are more accurate than their MRTD counterparts.

Index Terms—Finite-difference time-domain (FDTD), multiresolution time-domain (MRTD), numerical dispersion.

I. INTRODUCTION

FOR electrically large problems, the numerical dispersion inherent in the classical Yee finite-difference time-domain (FDTD) algorithm will introduce significant errors. Over the past ten years there have been several FDTD schemes published with the goal of reducing the dispersion error [1].

One of the simplest approaches to reducing the dispersion error is to retain more terms in the Taylor series approximation of the spatial derivatives than is done when using a second-order central difference. Because of the additional large storage requirements when applying a similar approach to the temporal derivatives, typically the standard second-order central differences are maintained in the approximation of the temporal derivatives. Fang [2] was the first to present this approach in conjunction with solving Maxwell's equations. He investigated the use of a second-order accurate in time, fourth-order accurate in space FDTD algorithm, which we denote as the (2, 4) FDTD algorithm. A few years later, Manry *et al.* [3] investigated the use of a second-order in time, sixth-order in space (2, 6) FDTD algorithm. More recently, Zhang and Chen [4] outlined a general procedure for generating the update-equation coefficients for arbitrary higher order (n, m) FDTD schemes. They also presented the corresponding dispersion relation for these schemes. The notation (n, m) denotes the order in accuracy of time and space of the FDTD scheme, respectively. In this paper, the $(2, m)$ higher order FDTD (HO-FDTD) schemes are considered.

In 1995, Krumpholz and Katehi introduced the multiresolution time-domain (MRTD) method, a time-domain scheme where electric and magnetic fields are expanded in terms of scaling and wavelet functions [5]. When using solely scaling functions, Krumpholz and Katehi termed the MRTD scheme an S-MRTD scheme, while when employing wavelet functions, they termed it a W-MRTD scheme. Krumpholz and Katehi primarily explored the use of Battle–Lemarie scaling functions, although other wavelet and scaling functions have since been used. Because Battle–Lemarie scaling functions suffer from the undesirable property of having noncompact support, other MRTD schemes have been proposed. Recently, Dogaru and Carin [6] proposed using Cohen–Daubechies–Feauveau (CDF) biorthogonal scaling and wavelet functions, while Wei *et al.* [7] proposed using Coifman scaling functions.

In Section II the three-dimensional (3-D) HO-FDTD update equations and dispersion relation are reviewed, while in Section III those of the S-MRTD are reviewed. The W-MRTD update equations and dispersion relation are presented in Section IV. Due to the complexity of the MRTD method when employing wavelet functions, the update equations and dispersion relation are presented solely in two dimensions (2-D) for the TM$_z$ case where the nonzero fields are E_z, H_x, and H_y. In Section V the dispersion errors of the HO-FDTD schemes are compared with the same size computational stencil S-MRTD schemes using either the CDF or Coifman scaling functions. When two schemes have the same spatial stencil and are run at the same Courant number, they require the same computational effort. The accuracy of all schemes is compared via direct evaluation of the dispersion relation governing each algorithm. For each scheme an "optimal" Courant number is determined that minimizes, or nearly minimizes, the dispersion error. Comparisons are made of the dispersion error when each scheme uses its own optimal Courant number. Additionally, comparisons are made when the HO-FDTD schemes are not optimized but rather use the Courant numbers that optimize the the MRTD scheme with the same stencil size. In Section VI the dispersion errors of the HO-FDTD schemes are compared with the CDF W-MRTD schemes requiring similar computational effort. Conclusions are presented in Section VII.

II. HIGHER ORDER FDTD SCHEMES

In 3-D the Cartesian coordinate higher order finite difference time-domain update equation for the z-component of the electric field can be obtained from (1) shown at the bottom of the next page

TABLE I
COEFFICIENTS FOR THE HIGHER ORDER FDTD SCHEMES

	HO-FDTD $(2,6)$	HO-FDTD $(2,10)$	HO-FDTD $(2,12)$	HO-FDTD $(2,14)$	HO-FDTD $(2,16)$
$a(1)$	1.171875000	1.211242676	1.22133636	1.228606224	1.23409107
$a(2)$	$-6.510416677 \times 10^{-2}$	$-8.97216797 \times 10^{-2}$	$-9.69314575 \times 10^{-2}$	-0.102383852	-0.106649846
$a(3)$	$4.687500000 \times 10^{-3}$	$1.38427734 \times 10^{-2}$	$1.74476624 \times 10^{-2}$	$2.04767704 \times 10^{-2}$	$2.30363667 \times 10^{-2}$
$a(4)$		$-1.76565988 \times 10^{-3}$	$-2.96728952 \times 10^{-3}$	$-4.17893273 \times 10^{-3}$	$-5.34238560 \times 10^{-3}$
$a(5)$		$1.18679470 \times 10^{-4}$	$3.59005398 \times 10^{-4}$	$6.89453549 \times 10^{-4}$	$1.07727117 \times 10^{-3}$
$a(6)$			$-2.18478116 \times 10^{-5}$	$-7.69225034 \times 10^{-5}$	$-1.66418878 \times 10^{-4}$
$a(7)$				$4.23651475 \times 10^{-6}$	$1.70217111 \times 10^{-5}$
$a(8)$					$-8.52346421 \times 10^{-7}$

where n_a is half the size of the total number of terms in the computational stencil, Δt is the temporal step size, Δx and Δy are the spatial step sizes in the x- and y-directions, respectively, ϵ is the permittivity, and the coefficients $a(\ell)$ are given in Table I. Similar equations hold for the other five field components and can be found in the Appendix. Note that Table I only includes coefficients that correspond to the same size stencil as either the CDF or Coifman S-MRTD schemes, which will be considered in Section V.

The dispersion characteristics are typically derived by assuming a time harmonic plane-wave solution in an isotropic, homogeneous, linear, and lossless medium. The dispersion relation for the higher order FDTD scheme can be written as

$$\frac{1}{c^2}\left[d_t(\Omega)\right]^2 = \left[F_x\left(\tilde{k}_x\delta\right)\right]^2 + \left[F_y\left(\tilde{k}_y\delta\right)\right]^2 + \left[F_z\left(\tilde{k}_z\delta\right)\right]^2 \quad (2)$$

where

$$d_t(\Omega) = \frac{1}{\Delta t}\sin\left(\frac{\omega\Delta t}{2}\right) \quad (3)$$

$$F_x\left(\tilde{k}_x\delta\right) = \frac{1}{\delta}\sum_{\ell=1}^{n_a} a(\ell)\sin\left(\frac{\tilde{k}_x(2\ell-1)\delta}{2}\right) \quad (4)$$

$$F_y\left(\tilde{k}_y\delta\right) = \frac{1}{\delta}\sum_{\ell=1}^{n_a} a(\ell)\sin\left(\frac{\tilde{k}_y(2\ell-1)\delta}{2}\right) \quad (5)$$

$$F_z\left(\tilde{k}_z\delta\right) = \frac{1}{\delta}\sum_{\ell=1}^{n_a} a(\ell)\sin\left(\frac{\tilde{k}_z(2\ell-1)\delta}{2}\right) \quad (6)$$

ω is the frequency, $\tilde{k}_\xi, \xi \in \{x, y, z\}$, is the numeric wave number in the x-, y-, and z-directions, respectively, and we have assumed a uniform spatial step size where $\Delta x = \Delta y = \Delta z = \delta$. For a given number of cells per wavelength N_λ, Courant number $S = c\Delta t/\delta$, and direction of propagation specified by the spherical polar angle θ and the equatorial angle φ, the arguments of each of the terms in (3)–(6) can be rewritten such that the only unknown is the ratio of the exact wavelength λ (i.e., the wavelength in the continuous world) to the numeric wavelength $\tilde{\lambda}$. (For example, the argument $\omega\Delta t/2$ can be rewritten as $\pi S/N_\lambda$, while $\tilde{k}_x(2\ell - 1)\delta/2$ could be expressed as $(\pi/N_\lambda)\cos\varphi\sin\theta(2\ell - 1)(\lambda/\tilde{\lambda})$.) The quantity $\lambda/\tilde{\lambda}$ can be solved numerically using techniques such as bisection. The dispersion error per wavelength, as later shown in Figs. 2–10, is then $360°(\lambda/\tilde{\lambda}-1)$.

III. SCALING-FUNCTION-BASED MRTD SCHEMES

In the 3-D scaling-function-based MRTD (S-MRTD) technique, the field at a point is a weighted sum of scaling functions. For example, the z-component of the electric field is given by

$$E_z(x, y, z, t)$$
$$= \sum_{n,i,j,k=-\infty}^{\infty} {}_nE^{z,\phi}_{i,j,k+(1/2)}h_n(t)\phi_i(x)\phi_j(y)\phi_{k+(1/2)}(z) \quad (7)$$

where ϕ is the appropriate scaling function for the particular scheme being used, h is a rectangular pulse function, and ${}_nE^{z,\phi}_{i,j,k+(1/2)}$ is the scaling-function coefficient. Rather than updating the fields directly, one updates the coefficients for the scaling functions. For example, from the z-component of Ampere's law, one obtains (8) shown at the bottom of the page, where n_a is again half the size of the computational

$$\frac{\epsilon}{\Delta t}\left(E^{z,n+1}_{i,j,k+(1/2)} - E^{z,n}_{i,j,k+(1/2)}\right)$$
$$= \sum_{\ell=1}^{n_a} a(\ell)\left[\frac{1}{\Delta x}\left(H^{y,n+(1/2)}_{i+\ell-(1/2),j,k+(1/2)} - H^{y,n+(1/2)}_{i-\ell+(1/2),j,k+(1/2)}\right) - \frac{1}{\Delta y}\left(H^{x,n+(1/2)}_{i,j+\ell-(1/2),k+(1/2)} - H^{x,n+(1/2)}_{i,j-\ell+(1/2),k+(1/2)}\right)\right] \quad (1)$$

$$\frac{\epsilon}{\Delta t}\left({}_{n+1}E^{z,\phi}_{i,j,k+(1/2)} - {}_nE^{z,\phi}_{i,j,k+(1/2)}\right)$$
$$= \sum_{\ell=1}^{n_a} a(\ell)\left[\frac{1}{\Delta x}\left({}_{n+(1/2)}H^{y,\phi}_{i+\ell-(1/2),j,k+(1/2)} - {}_{n+(1/2)}H^{y,\phi}_{i-\ell+(1/2),j,k+(1/2)}\right)\right.$$
$$\left. - \frac{1}{\Delta y}\left({}_{n+(1/2)}H^{x,\phi}_{i,j+\ell-(1/2),k+(1/2)} - {}_{n+(1/2)}H^{x,\phi}_{i,j-\ell+(1/2),k+(1/2)}\right)\right] \quad (8)$$

TABLE II
COEFFICIENTS FOR THE S-MRTD SCHEMES.

	CDF $(2, 2)$	CDF $(2, 4)$	CDF $(2, 6)$	Coifman-4	Coifman-8
$a(1)$	1.2291666667	1.2918129281	1.3110340773	1.31176	1.30666
$a(2)$	-0.0937500000	-0.1371343465	-0.1560100710	-0.15757	-0.16494
$a(3)$	0.0104166667	0.0287617723	0.0419957460	0.04383	0.06042
$a(4)$		-0.0034701413	-0.0086543236	-0.00982	-0.02429
$a(5)$		0.0000080265	0.0008308695	0.00124	0.00857
$a(6)$			0.0000108999	-0.00005	-0.00243
$a(7)$			-0.0000000041		0.00053
$a(8)$					-0.00009

stencil, and the coefficients $a(\ell)$ are given in Table II for the CDF schemes $(2, 2)$, $(2, 4)$, and $(2, 6)$ and Coifman-4 and -8 schemes. The Coifman coefficients are as given in [7]. Note the similarity between (8) and (1). This similarity holds for the update equations for the other scaling-function coefficients, and hence they will not be shown.

Unlike the HO-FDTD schemes, for the CDF schemes the (α, β) notation relates to the lengths of the reconstruction and decomposition filters of the wavelet family. By comparing the number of coefficients used in each algorithm, it can be seen that the HO-FDTD $(2, 6)$ scheme has the same computational stencil as the CDF $(2, 2)$ S-MRTD scheme, the HO-FDTD $(2, 10)$ scheme has the same computational stencil as the CDF $(2, 4)$ scheme, the HO-FDTD $(2, 14)$ scheme has the same stencil as the CDF $(2, 6)$ scheme, the HO-FDTD $(2, 12)$ scheme has the same stencil as the Coifman-4 scheme, and the HO-FDTD $(2, 16)$ scheme has the same stencil as the Coifman-8 scheme. Thus, these combinations of schemes will be compared in Section V.

The dispersion relation for the S-MRTD scheme is essentially identical to that of the HO-FDTD scheme except the coefficients used in (4)–(6) would be taken from Table II instead of Table I.

IV. WAVELET-FUNCTION-BASED MRTD SCHEMES

Due to the complexity of wavelet-based MRTD schemes, we limit our discussion of the W-MRTD CDF schemes to

2-D TM$_z$ polarization where the nonzero fields are E_z, H_x, and H_y. The z-component of the electric field is represented by the expansion shown in (9) at the bottom of the page [6], [8], while the x- and y-components of the magnetic field are given by (10)–(11) shown at the bottom of the page, where $\tilde{\Phi}$ is the dual scaling function and $\tilde{\Psi}$ is the corresponding dual wavelet. The arrangement of the basis function coefficients is shown in Fig. 1.

The update equation for the $\Phi\Phi$ basis function coefficient for E_z can be obtained from (12) shown at the bottom of the next page, where n_c is half of the total size of the spatial stencils involving the c coefficients. As shown in the Appendix, similar expressions hold for the remaining basis function coefficient updates. Equation (12) utilizes the two sets of coefficients $a(\ell)$ and $c(\ell)$. As shown in the Appendix, two other sets of coefficients, namely, $b(\ell)$ and $d(\ell)$, are required in the complete set of 2-D W-MRTD update equations. For completeness the coefficients $b(\ell)$, $c(\ell)$, and $d(\ell)$ as given in [6] are shown in Table III for the CDF $(2, 2)$, $(2, 4)$, and $(2, 6)$ schemes. The $a(\ell)$ coefficients are simply those given in Table II.

The equations governing the update of the magnetic field basis function coefficients are also given in the Appendix. Note that the S-MRTD scheme is recovered if only the $\phi\phi$ terms are retained.

The dispersion relation for the 2-D W-MRTD scheme can be shown to be given by setting the determinant of a 12×12 matrix

$$
\begin{aligned}
E_z&(x, y, t) \\
&= \sum_{n,i,j=-\infty}^{\infty} \left[{}_n E_{i,j}^{z,\phi\phi} \tilde{\Phi}_i(x)\tilde{\Phi}_j(y) + {}_n E_{i,j+(1/2)}^{z,\phi\psi} \tilde{\Phi}_i(x)\tilde{\Psi}_{j+(1/2)}(y) \right. \\
&\quad \left. + {}_n E_{i+(1/2),j}^{z,\psi\phi} \tilde{\Psi}_{i+(1/2)}(x)\tilde{\Phi}_j(y) + {}_n E_{i+(1/2),j+(1/2)}^{z,\psi\psi} \tilde{\Psi}_{i+(1/2)}(x)\tilde{\Psi}_{j+(1/2)}(y) \right] h_n(t)
\end{aligned}
\tag{9}
$$

$$
\begin{aligned}
H_x(x, y, t) &= \sum_{n,i,j=-\infty}^{\infty} \left[{}_{n+(1/2)} H_{i,j+(1/2)}^{x,\phi\phi} \tilde{\Phi}_i(x)\tilde{\Phi}_{j+(1/2)}(y) + {}_{n+(1/2)} H_{i,j}^{x,\phi\psi} \tilde{\Phi}_i(x)\tilde{\Psi}_j(y) \right. \\
&\quad \left. + {}_{n+(1/2)} H_{i+(1/2),j+(1/2)}^{x,\psi\phi} \tilde{\Psi}_{i+(1/2)}(x)\tilde{\Phi}_{j+(1/2)}(y) + {}_{n+(1/2)} H_{i+(1/2),j}^{x,\psi\psi} \tilde{\Psi}_{i+(1/2)}(x)\tilde{\Psi}_j(y) \right] h_{n+(1/2)}(t)
\end{aligned}
\tag{10}
$$

$$
\begin{aligned}
H_y(x, y, t) &= \sum_{n,i,j=-\infty}^{\infty} \left[{}_{n+(1/2)} H_{i+(1/2),j}^{y,\phi\phi} \tilde{\Phi}_{i+(1/2)}(x)\tilde{\Phi}_j(y) + {}_{n+(1/2)} H_{i+(1/2),j+(1/2)}^{y,\phi\psi} \tilde{\Phi}_{i+(1/2)}(x)\tilde{\Psi}_{j+(1/2)}(y) \right. \\
&\quad \left. + {}_{n+(1/2)} H_{i,j}^{y,\psi\phi} \tilde{\Psi}_i(x)\tilde{\Phi}_j(y) + {}_{n+(1/2)} H_{i,j+(1/2)}^{y,\psi\psi} \tilde{\Psi}_i(x)\tilde{\Psi}_{j+(1/2)}(y) \right] h_{n+(1/2)}(t)
\end{aligned}
\tag{11}
$$

$$
\begin{array}{ccc}
_nE^{z,\phi\phi}_{i,j+1} & _nE^{z,\psi\phi}_{i+\frac{1}{2},j+1} & _nE^{z,\phi\phi}_{i+1,j+1} \\[2pt]
\bullet\;\; _{n+\frac{1}{2}}H^{y,\psi\phi}_{i,j+1} & \circ\;\; _{n+\frac{1}{2}}H^{x,\psi\psi}_{i+\frac{1}{2},j+1} & \bullet\;\; _{n+\frac{1}{2}}H^{x,\phi\psi}_{i+1,j+1} \\[2pt]
_{n+\frac{1}{2}}H^{x,\phi\psi}_{i,j+1} & _{n+\frac{1}{2}}H^{y,\phi\phi}_{i+\frac{1}{2},j+1} & _{n+\frac{1}{2}}H^{y,\psi\phi}_{i+1,j+1} \\[8pt]
_nE^{z,\phi\psi}_{i,j+\frac{1}{2}} & _nE^{z,\psi\psi}_{i+\frac{1}{2},j+\frac{1}{2}} & _nE^{z,\phi\psi}_{i+1,j+\frac{1}{2}} \\[2pt]
\square\;\; _{n+\frac{1}{2}}H^{x,\phi\phi}_{i,j+\frac{1}{2}} & \boxplus\;\; _{n+\frac{1}{2}}H^{x,\psi\phi}_{i+\frac{1}{2},j+\frac{1}{2}} & \square\;\; _{n+\frac{1}{2}}H^{x,\phi\phi}_{i+1,j+\frac{1}{2}} \\[2pt]
_{n+\frac{1}{2}}H^{y,\psi\psi}_{i,j+\frac{1}{2}} & _{n+\frac{1}{2}}H^{y,\phi\psi}_{i+\frac{1}{2},j+\frac{1}{2}} & _{n+\frac{1}{2}}H^{y,\psi\psi}_{i+1,j+\frac{1}{2}} \\[8pt]
_nE^{z,\phi\phi}_{i,j} & _nE^{z,\psi\phi}_{i+\frac{1}{2},j} & _nE^{z,\phi\phi}_{i+1,j} \\[2pt]
\bullet\;\; _{n+\frac{1}{2}}H^{x,\phi\psi}_{i,j} & \circ\;\; _{n+\frac{1}{2}}H^{x,\psi\psi}_{i+\frac{1}{2},j} & \bullet\;\; _{n+\frac{1}{2}}H^{x,\phi\psi}_{i+1,j} \\[2pt]
_{n+\frac{1}{2}}H^{y,\psi\phi}_{i,j} & _{n+\frac{1}{2}}H^{y,\phi\phi}_{i+\frac{1}{2},j} & _{n+\frac{1}{2}}H^{y,\psi\phi}_{i+1,j}
\end{array}
$$

Fig. 1. Arrangement of basis-function coefficients in the W-MRTD grid.

TABLE III
THE $b(\ell)$, $c(\ell)$, AND $d(\ell)$ COEFFICIENTS FOR THE CDF W-MRTD SCHEME

	CDF (2, 2)	CDF (2, 4)	CDF (2, 6)
$b(1)$	1.4375000	1.6890090	1.8610039
$b(2)$	0.0937500	0.1955818	0.2903309
$b(3)$	−0.0104167	−0.0267622	−0.0426845
$b(4)$		0.0034701	0.0086545
$b(5)$		−0.0000080	−0.0008308
$b(6)$			−0.0000109
$c(1)$	−0.1510417	−0.1569410	−0.1390804
$c(2)$	0.0833333	0.1363198	0.1482517
$c(3)$	−0.0052083	−0.0443966	−0.0742472
$c(4)$		0.0047841	0.0192157
$c(5)$		−0.0003301	−0.0026345
$c(6)$		0.0000008	0.0002887
$c(7)$			−0.0000146
$c(8)$			−0.0000002
$d(1)$	−0.0416667	−0.0726900	−0.0954514
$d(2)$	0.0208333	0.0364721	0.0468862
$d(3)$		−0.0000856	0.0005564
$d(4)$			−0.0000002

to zero. That matrix is given by (13) shown at the bottom of the page, where, assuming $\Delta x = \Delta y = \delta$

$$
C_{\xi\zeta} = \sum_{\ell} \frac{\xi(\ell)\sin\left(k_\zeta\left(\ell-\frac{1}{2}\right)\delta\right)}{\sin\left(\frac{\omega\Delta t}{2}\right)}\frac{\Delta t}{\delta} \quad \xi \in \{a,b\},\ \zeta \in \{x,y\}
\tag{14}
$$

$$
C_{\xi\zeta} = \sum_{\ell} \frac{\xi(\ell)\sin\left(k_\zeta\ell\delta\right)}{\sin\left(\frac{\omega\Delta t}{2}\right)}\frac{\Delta t}{\delta} \quad \xi \in \{c,d\},\ \zeta \in \{x,y\}.
\tag{15}
$$

Prior to expanding the $C_{\xi\zeta}$ terms, the determinant was found symbolically using *Mathematica* [9]. The $C_{\xi\zeta}$ terms were then expanded in accordance with (14) and (15) and, as before, the resulting equation was solved numerically for the ratio $\lambda/\tilde{\lambda}$, which was then used to obtain the dispersion error per wavelength.

V. COMPARISONS BETWEEN HIGHER ORDER FDTD AND S-MRTD-BASED SCHEMES

Fig. 2 shows the maximum numerical dispersion error in 3-D (evaluated over all propagation angles) versus the Courant number for the (2, 6), (2, 10), and (2, 14) HO-FDTD schemes as well as for the S-MRTD schemes with the same size spatial stencil, namely, the CDF (2, 2), CDF (2, 4), and CDF (2, 6)

$$
\begin{aligned}
&\frac{\epsilon}{\Delta t}\left(_{n+1}E^{z,\phi\phi}_{i,j} - {_n}E^{z,\phi\phi}_{i,j}\right) \\
&= \sum_{\ell=1}^{n_a} a(\ell)\left[\frac{1}{\Delta x}\left(_{n+(1/2)}H^{y,\phi\phi}_{i+\ell-(1/2),j} - {_{n+(1/2)}}H^{y,\phi\phi}_{i-\ell+(1/2),j}\right) - \frac{1}{\Delta y}\left(_{n+(1/2)}H^{x,\phi\phi}_{i,j+\ell-(1/2)} - {_{n+(1/2)}}H^{x,\phi\phi}_{i,j-\ell+(1/2)}\right)\right] \\
&\quad + \sum_{\ell=1}^{n_c} c(\ell)\left[\frac{1}{\Delta x}\left(_{n+(1/2)}H^{y,\psi\phi}_{i+\ell,j} - {_{n+(1/2)}}H^{y,\psi\phi}_{i-\ell,j}\right) - \frac{1}{\Delta y}\left(_{n+(1/2)}H^{x,\phi\psi}_{i,j+\ell} - {_{n+(1/2)}}H^{x,\phi\psi}_{i,j-\ell}\right)\right]
\end{aligned}
\tag{12}
$$

$$
\begin{bmatrix}
\epsilon & 0 & 0 & 0 & -C_{ay} & 0 & -C_{cy} & 0 & C_{ax} & 0 & 0 & C_{cx} \\
0 & \epsilon & 0 & 0 & 0 & -C_{by} & 0 & -C_{dy} & 0 & C_{bx} & C_{dx} & 0 \\
0 & 0 & \epsilon & 0 & -C_{dy} & 0 & -C_{by} & 0 & 0 & C_{cx} & C_{ax} & 0 \\
0 & 0 & 0 & \epsilon & 0 & -C_{cy} & 0 & -C_{ay} & C_{dx} & 0 & 0 & C_{bx} \\
-C_{ax} & 0 & -C_{cy} & 0 & \mu & 0 & 0 & 0 & 0 & 0 & 0 & 0 \\
0 & -C_{by} & 0 & -C_{dy} & 0 & \mu & 0 & 0 & 0 & 0 & 0 & 0 \\
-C_{dy} & 0 & -C_{by} & 0 & 0 & 0 & \mu & 0 & 0 & 0 & 0 & 0 \\
0 & -C_{cy} & 0 & -C_{ay} & 0 & 0 & 0 & \mu & 0 & 0 & 0 & 0 \\
C_{ax} & 0 & 0 & C_{cx} & 0 & 0 & 0 & 0 & \mu & 0 & 0 & 0 \\
0 & C_{bx} & C_{dx} & 0 & 0 & 0 & 0 & 0 & 0 & \mu & 0 & 0 \\
0 & C_{cx} & C_{ax} & 0 & 0 & 0 & 0 & 0 & 0 & 0 & \mu & 0 \\
C_{dx} & 0 & 0 & C_{bx} & 0 & 0 & 0 & 0 & 0 & 0 & 0 & \mu
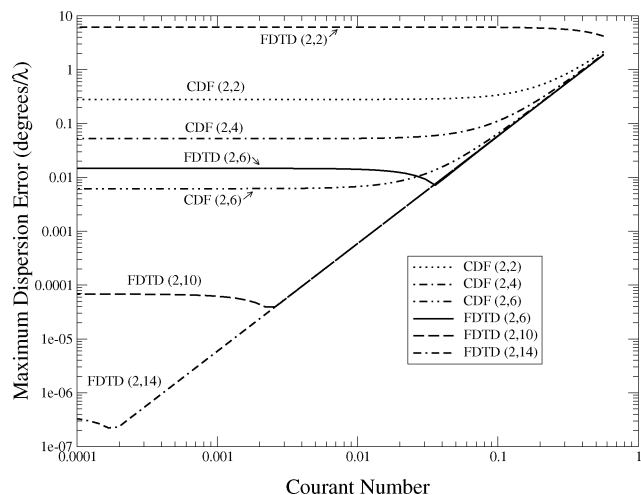\end{bmatrix}
\tag{13}
$$

Fig. 2. Dispersion error versus Courant number for three HO-FDTD schemes and the CDF S-MRTD schemes with the same spatial stencils. The discretization is held fixed at ten cells per wavelength. As a point of reference, the dispersion for the FDTD (2, 2) scheme, i.e., the classic Yee algorithm, is shown as the dashed line that appears at the top of the plot.
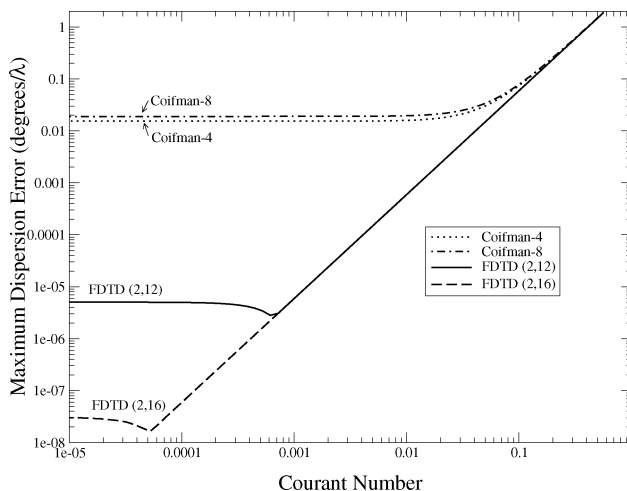

Fig. 3. Dispersion error versus Courant number for two HO-FDTD schemes and the Coifman S-MRTD schemes with the same spatial stencils. The discretization is held fixed at ten cells per wavelength.

TABLE IV
COURANT NUMBERS THAT OPTIMIZE THE VARIOUS SCHEMES AT TEN CELLS PER WAVELENGTH. THE SCHEMES ARE GROUPED ACCORDING TO THEIR SPATIAL STENCIL SIZE (THE MULTIPLICITY OF THE W-MRTD STENCILS NOTWITHSTANDING)

HO-FDTD $(2, 6)$	0.03568
S-MRTD CDF $(2, 2)$	0.1541
W-MRTD CDF $(2, 2)$	0.1110
HO-FDTD $(2, 10)$	0.002200
S-MRTD CDF $(2, 4)$	0.06553
W-MRTD CDF $(2, 4)$	0.01760
HO-FDTD $(2, 14)$	0.0001876
S-MRTD CDF $(2, 6)$	0.02309
W-MRTD CDF $(2, 6)$	0.02100
HO-FDTD $(2, 12)$	0.0006813
Coifman-4	0.03600
HO-FDTD $(2, 16)$	0.00005196
Coifman-8	0.03994

schemes, respectively. The error is defined as the absolute value of the phase error in degrees per wavelength of propagation. Each scheme is evaluated at a resolution of ten cells per λ ($N_\lambda = 10$). The HO-FDTD schemes can, depending on the Courant number, yield propagation that is either faster or slower than the speed of light. The optimal Courant number occurs at the distinct dip in each HO-FDTD curve. At this Courant number the mean of the dispersion error (with the sign preserved) is zero when measured over all propagation directions. The errors from the CDF S-MRTD schemes are seen to decrease asymptotically with decreasing Courant number. Note that the HO-FDTD schemes have lower dispersion than the corresponding S-MRTD scheme. In fact the HO-FDTD error can be several orders of magnitude less than the S-MRTD error. However, to realize such performance in the HO-FDTD methods the Courant number would have to be so small that it essentially precludes practical use. Therefore, later in this section comparisons will be made using a common Courant number.

Fig. 3 shows the maximum numerical 3-D dispersion error versus Courant number for the (2, 12) and (2, 16) HO-FDTD schemes and their S-MRTD counterparts with the same size spatial stencils; namely, the Coifman-4 and Coifman-8 S-MRTD schemes, respectively. Again, each scheme is evaluated at a resolution of ten cells per λ. Once again, the errors from the Coifman S-MRTD schemes are seen to decrease asymptotically with decreasing Courant number. Similarly, the HO-FDTD schemes are capable of producing significantly lower levels of error at small Courant numbers. However, as noted before, the Courant numbers required to produce this level of performance are so small that they preclude use in most applications.

For the remaining plots in this section, in each S-MRTD scheme we will use a Courant number that yields a maximum error that is 1.5 times the asymptotic limit of error for that particular scheme. Thus, the Courant number is reasonably large while still yielding errors close to the asymptotic limit. We

denote this as the "optimal" Courant number for the S-MRTD scheme. The optimal Courant numbers for the S-MRTD schemes are typically much larger than the optimal Courant number for the corresponding HO-FDTD scheme. The optimal Courant numbers used in this work are listed in Table IV.

Fig. 4 shows the maximum dispersion error versus the cells per wavelength for the three CDF S-MRTD schemes and the HO-FDTD schemes when each uses a time-step that optimizes its performance at ten cells per wavelength, i.e., each scheme uses the Courant number given in Table IV. The HO-FDTD schemes are clearly superior to their corresponding CDF S-MRTD counterparts, although to achieve this superiority the HO-FDTD schemes require a much smaller Courant number. In fact, the size of the Courant number for the HO-FDTD schemes is so small as to be prohibitive, and thus these curves serve primarily to show the lower bound on the error. Fig. 5 shows the same set of plots, but comparing the HO-FDTD
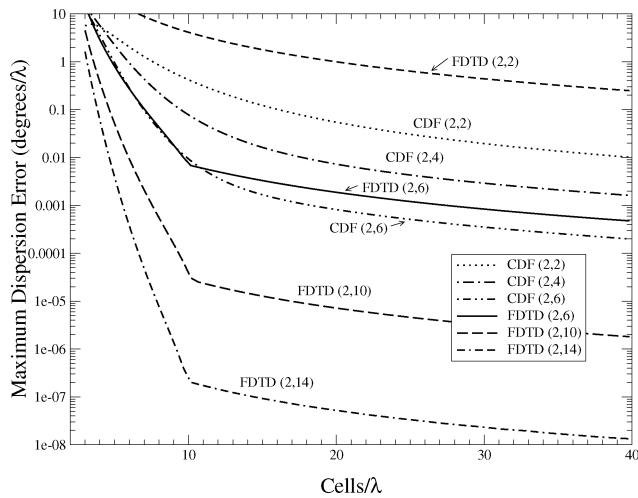
Fig. 4. Dispersion error versus cells per wavelength for three HO-FDTD schemes and the CDF S-MRTD schemes with the same spatial stencils. The Courant number for each scheme is the one which optimizes the performance at ten cells per wavelength. Again, for reference, the dispersion for the FDTD (2, 2) scheme is shown as the dashed line appearing at the top of the plot.
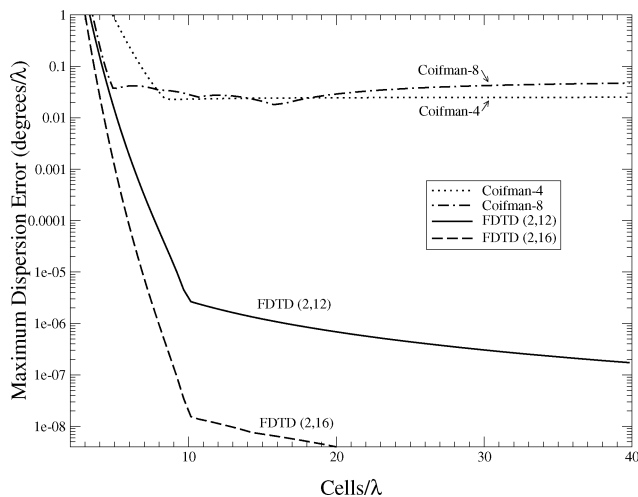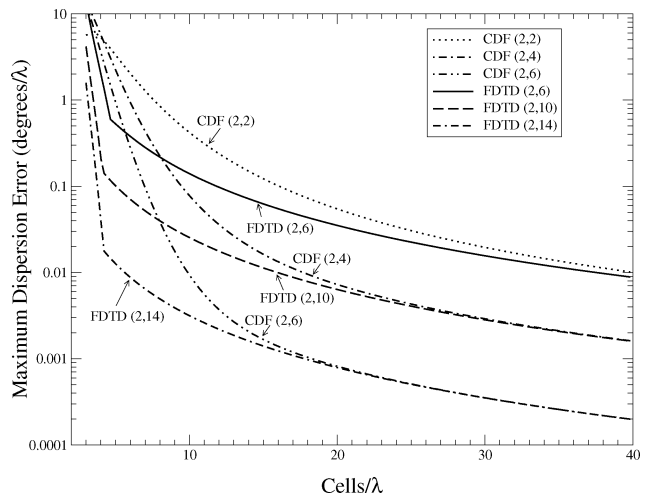

Fig. 6. Dispersion error versus cells per wavelength. Here the HO-FDTD schemes use the Courant numbers that are optimum for the corresponding CDF S-MRTD schemes.
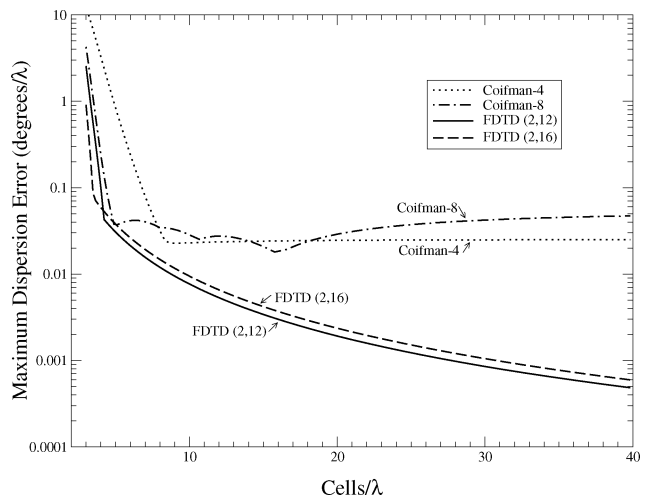

Fig. 5. Dispersion error versus cells per wavelength for two HO-FDTD schemes and the Coifman S-MRTD schemes with the same spatial stencils. The Courant number for each scheme is the one that optimizes the performance at ten cells per wavelength.

Fig. 7. Dispersion error versus cells per wavelength. The HO-FDTD schemes use the Courant numbers that are optimum for the Coifman S-MRTD schemes.

schemes with their Coifman S-MRTD counterparts. The same conclusions are drawn. (We note that some improvement in the Coifman results may be possible if more digits were used in the update coefficients than those provided by [7], but results are not likely to be significantly different.).

Fig. 6 again shows the maximum dispersion versus discretization; however, here the HO-FDTD schemes use the Courant number that optimizes the CDF S-MRTD scheme with the same spatial stencil. Because the S-MRTD and HO-FDTD schemes use the same Courant numbers and have the same spatial stencils, they require the same computational effort. Using this larger Courant number, the HO-FDTD schemes are still superior to S-MRTD at coarse discretizations while S-MRTD converges to the HO-FDTD error as the discretization becomes more fine. Fig. 7 shows that the HO-FDTD schemes

are superior to the Coifman S-MRTD schemes over all discretizations.

Finally, note that the plots have shown only the maximum error when considering all propagation angles. If a scheme has the same dispersion error at all angles, the scheme is isotropic. For such a scheme it may be possible via postprocessing to remove the dispersion error even if that error is large. In practice all schemes suffer some anisotropy, but if the anisotropy is small relative to the mean dispersion error, postprocessing may be used to remove the mean error and thus significantly improve the quality of the results. Thus, it is instructive to determine the degree of anisotropy for each of the schemes, or, said another way, the difference between the dispersion in the direction with most error and the dispersion in the direction with least error. Table V shows this anisotropy for each of the schemes at ten cells per wavelength when using the Courant numbers, which optimize the S-MRTD schemes at this discretization. Again the schemes are grouped by their spatial stencil size. In all cases the HO-FDTD schemes are much more isotropic than the corresponding S-MRTD scheme.

TABLE V
DEGREE OF ANISOTROPY AT TEN CELLS PER WAVELENGTH FOR THE
HO-FDTD AND S-MRTD SCHEMES WHEN EACH SCHEME USES THE
COURANT NUMBER WHICH OPTIMIZES THE PERFORMANCE OF THE MRTD
SCHEME. THE DEGREE OF ANISOTROPY IS DEFINED AS THE ABSOLUTE VALUE
OF THE DIFFERENCE BETWEEN THE MAXIMUM AND MINIMUM ERRORS
(WHERE SIGN IS PRESERVED IN DETERMINING THE MINIMUM AND MAXIMUM)
WHEN MEASURED OVER ALL PROPAGATION ANGLES. HENCE THE SMALLER
THE NUMBER, THE MORE ISOTROPIC THE ALGORITHM IS

HO-FDTD $(2, 6)$	0.01415
S-MRTD CDF $(2, 2)$	0.2456
HO-FDTD $(2, 10)$	6.759×10^{-5}
S-MRTD CDF $(2, 4)$	5.018×10^{-2}
HO-FDTD $(2, 14)$	3.882×10^{-7}
S-MRTD CDF $(2, 6)$	6.084×10^{-3}
HO-FDTD $(2, 12)$	5.039×10^{-6}
Coifman-4	0.01060
HO-FDTD $(2, 16)$	3.090×10^{-8}
Coifman-8	0.01030

Fig. 9. Dispersion error versus cells per wavelength for three HO-FDTD schemes and the CDF W-MRTD schemes with the same spatial stencils. The Courant number for each scheme optimizes its performance at 10 cells per wavelength.
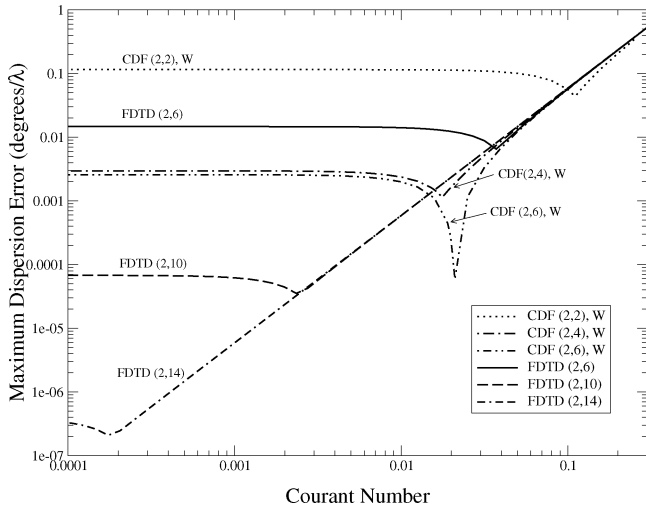

Fig. 8. Dispersion error versus Courant number for three HO-FDTD schemes and the CDF W-MRTD schemes with the same spatial stencils. The discretization is held fixed at 10 cells per wavelength.

Fig. 10. Dispersion error versus cells per wavelength for three HO-FDTD schemes and the CDF W-MRTD schemes with the same spatial stencils. The Courant number for each CDF scheme optimizes its performance at 10 cells per wavelength. For the HO-FDTD the Courant number is that which yields the same "computational effort" as the CDF scheme with the same size spatial stencil.

VI. COMPARISONS BETWEEN HIGHER ORDER FDTD AND W-MRTD SCHEMES

Fig. 8 shows the maximum 2-D dispersion error versus Courant number for the three CDF W-MRTD schemes and their three 2-D HO-FDTD counterparts. Note that unlike the S-MRTD schemes, the W-MRTD schemes have a well-defined optimum Courant number. Fig. 9 shows the maximum dispersion error versus discretization for all six schemes when each scheme uses the Courant number that optimizes its performance at ten cells per λ.

Fig. 10 also shows the maximum dispersion error versus discretization. Once again, the W-MRTD results were obtained using the Courant numbers that optimize their performance at ten cells per λ. The same caveat concerning the small Courant numbers for the HO-FDTD schemes discussed in Section V pertains here as well.

By comparing the update equations for the W-MRTD method with those that govern the HO-FDTD or S-MRTD methods, it
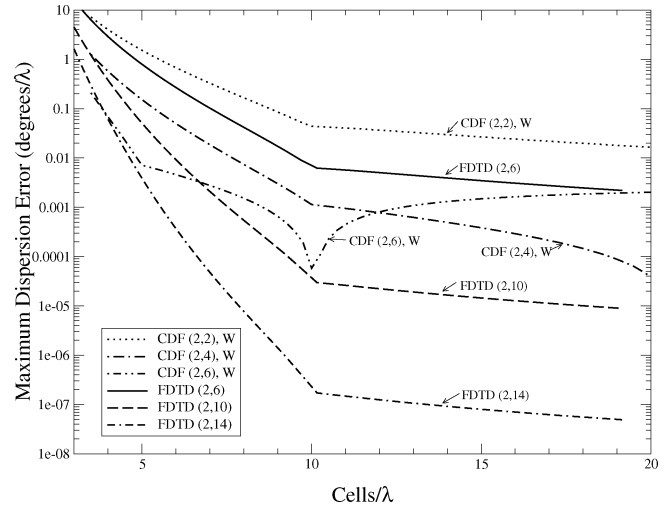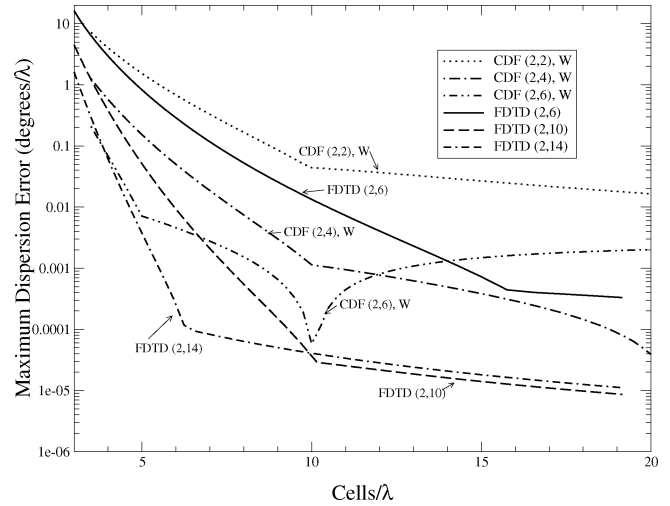
is evident that the W-MRTD method involves much more computation than either HO-FDTD or S-MRTD. This is because the update equations of the W-MRTD method typically involve summations over four sets of coefficients $a(\ell)$, $b(\ell)$, $c(\ell)$, and $d(\ell)$, while those of S-MRTD and HO-FDTD typically are over only one set of coefficients $a(\ell)$. (Under the assumption of equal stencils $a(\ell)$, $b(\ell)$, $c(\ell)$, and $d(\ell)$, this would be a factor of eight in computation.) Therefore, in Fig. 10, the HO-FDTD schemes use a Courant number that would result in approximately the same number of computations (and hence run time) as the corresponding W-MRTD scheme. For example, in the TE_z polarization case, to update the E_z CDF $(2, 2)$ field component requires four stencils of size $n_a = 3$, $n_b = 3$, $n_c = 3$, and $n_d = 2$, while the HO-FDTD $(2, 6)$ simply utilizes two of size $n_a = 3$. Similar ratios of operation counts exist between the H_x and H_y

field components for the two schemes. The stencil size is proportional to the floating point operation count; thus the CDF (2, 2) W-MRTD results in 44/6 as many operations per time step as the HO-FDTD. Therefore, using an FDTD Courant number 3/22 that of the CDF (2, 2) W-MRTD scheme results in the same amount of computation. This is the HO-FDTD Courant number used in the HO-FDTD (2, 6) case. Similarly, for the HO-FDTD (2, 10) results shown in Fig. 10, a Courant number 5/38 that of the CDF (2, 4) W-MRTD is used. Lastly, for HO-FDTD (2, 14), a Courant number 1/8 that of CDF (2, 6) is used in Fig. 10. As can be seen from Fig. 10, except perhaps over a very small range of discretizations, HO-FDTD (2, 6) has better dispersion than CDF (2, 2) W-MRTD, HO-FDTD (2, 10) performs better than CDF (2, 4) W-MRTD, and HO-FDTD (2, 14) performs better than CDF (2, 6) W-MRTD.

From Table IV it is observed that at ten cells per wavelength the optimum Courant number for the CDF (2, 2) W-MRTD scheme is 0.1110 while for the HO-FDTD (2, 6) scheme it is 0.035 68. Taking the optimum W-MRTD Courant number and reducing it by a factor of 3/22 yields a Courant number of 0.015 14. Note that this Courant number is *less than* the one that yields optimum behavior at ten cells per wavelength for the HO-FDTD (2, 6) scheme. Nevertheless, since, as is evident from Fig. 8, the suboptimal Courant number does not significantly degrade the performance of the HO-FDTD (2, 6) scheme and since this Courant number does yield the same computational effort as the W-MRTD scheme, it is the Courant number used in Fig. 10. Reducing the Courant number from the value that optimizes the performance at ten cells per wavelength merely changes the discretization at which the behavior is optimum (from Fig. 10 it appears the smaller Courant number provides optimum behavior near 16 cells per wavelength). If one were truly interested in optimizing behavior at ten cells

per wavelength, a Courant number of 0.035 68 could be used for the HO-FDTD (2, 6) scheme. In that case the curve shown in Fig. 9 is the pertinent one and the HO-FDTD (2, 6) scheme would require less computational effort than the corresponding optimized W-MRTD scheme.

VII. CONCLUSION

Comparisons in accuracy, due to numerical dispersion, have been made between higher order FDTD schemes and equivalent computational stencil MRTD schemes. The MRTD schemes investigated include the Cohen–Daubechies–Feauveau S-MRTD schemes, the Coifman S-MRTD schemes, and the CDF W-MRTD schemes. In all cases investigated, the HO-FDTD provides better dispersion characteristics than their corresponding MRTD counterparts, even when the HO-FDTD schemes utilize a Courant number that is optimal for the MRTD schemes. It is noted that our comparisons here solely compare the dispersion error of the various schemes in a homogeneous space. Easier implementation of an MRTD scheme over an HO-FDTD scheme due to difficulties at material interfaces may warrant MRTD usage over an HO-FDTD scheme.

APPENDIX

The equations that can be used to obtain the update equations for the remaining 3-D components of the HO-FDTD scheme are shown in (16)–(20) at the bottom of the page. The form of the equations is unchanged for the S-MRTD scheme—merely the value of the $a(\ell)$ coefficients changes.

For the 2-D W-MRTD TM_z polarization case, the remaining basis function coefficients for the z-component of the electric field can be updated using (21)–(23) shown at the top of next page.

$$\frac{\epsilon}{\Delta t}\left(E^{x,n+1}_{i+(1/2),j,k} - E^{x,n}_{i+(1/2),j,k}\right)$$
$$= \sum_{\ell=1}^{n_a} a(\ell)\left[\frac{1}{\Delta y}\left(H^{z,n+(1/2)}_{i+(1/2),j+\ell-(1/2),k} - H^{z,n+(1/2)}_{i+(1/2),j-\ell+(1/2),k}\right) - \frac{1}{\Delta z}\left(H^{y,n+(1/2)}_{i+(1/2),j,k+\ell-(1/2)} - H^{y,n+(1/2)}_{i+(1/2),j,k-\ell+(1/2)}\right)\right] \quad (16)$$

$$\frac{\epsilon}{\Delta t}\left(E^{y,n+1}_{i,j+(1/2),k} - E^{y,n}_{i,j+(1/2),k}\right)$$
$$= \sum_{\ell=1}^{n_a} a(\ell)\left[\frac{1}{\Delta z}\left(H^{x,n+(1/2)}_{i,j+(1/2),k+\ell-(1/2)} - H^{x,n+(1/2)}_{i,j+(1/2),k-\ell+(1/2)}\right) - \frac{1}{\Delta x}\left(H^{z,n+(1/2)}_{i+\ell-(1/2),j+(1/2),k} - H^{z,n+(1/2)}_{i-\ell+(1/2),j+(1/2),k}\right)\right] \quad (17)$$

$$\frac{\mu}{\Delta t}\left(H^{x,n+(1/2)}_{i,j+(1/2),k+(1/2)} - H^{x,n-(1/2)}_{i,j+(1/2),k+(1/2)}\right)$$
$$= \sum_{\ell=1}^{n_a} a(\ell)\left[\frac{1}{\Delta z}\left(E^{y,n}_{i,j+(1/2),k+\ell} - E^{y,n}_{i,j+(1/2),k-\ell+1}\right) - \frac{1}{\Delta y}\left(E^{z,n}_{i,j+\ell,k+(1/2)} - E^{z,n}_{i,j-\ell+1,k+(1/2)}\right)\right] \quad (18)$$

$$\frac{\mu}{\Delta t}\left(H^{y,n+(1/2)}_{i+(1/2),j,k+(1/2)} - H^{y,n-(1/2)}_{i+(1/2),j,k+(1/2)}\right)$$
$$= \sum_{\ell=1}^{n_a} a(\ell)\left[\frac{1}{\Delta x}\left(E^{z,n}_{i+\ell,j,k+(1/2)} - E^{z,n}_{i-\ell+1,j,k+(1/2)}\right) - \frac{1}{\Delta z}\left(E^{x,n}_{i+(1/2),j,k+\ell} - E^{x,n}_{i+(1/2),j,k-\ell+1}\right)\right] \quad (19)$$

$$\frac{\mu}{\Delta t}\left(H^{z,n+(1/2)}_{i+(1/2),j+(1/2),k} - H^{z,n-(1/2)}_{i+(1/2),j+(1/2),k}\right)$$
$$= \sum_{\ell=1}^{n_a} a(\ell)\left[\frac{1}{\Delta y}\left(E^{x,n}_{i+(1/2),j+\ell,k} - E^{x,n}_{i+(1/2),j-\ell+1,k}\right) - \frac{1}{\Delta x}\left(E^{y,n}_{i+\ell,j+(1/2),k} - E^{y,n}_{i-\ell+1,j+(1/2),k}\right)\right]. \quad (20)$$

$$\frac{\epsilon}{\Delta t}\left(_{n+1}E_{i,j+(1/2)}^{z,\phi\psi} - {_n}E_{i,j+(1/2)}^{z,\phi\psi}\right)$$

$$=\frac{1}{\Delta x}\sum_{\ell=1}^{n_a}a(\ell)\left(_{n+(1/2)}H_{i+\ell-(1/2),j+(1/2)}^{y,\phi\psi} - {_{n+(1/2)}}H_{i-\ell+(1/2),j+(1/2)}^{y,\phi\psi}\right) - \frac{1}{\Delta y}\sum_{\ell=1}^{n_b}b(\ell)\left(_{n+(1/2)}H_{i,j+\ell}^{x,\phi\psi} - {_{n+(1/2)}}H_{i,j-\ell+1}^{x,\phi\psi}\right)$$

$$+\frac{1}{\Delta x}\sum_{\ell=1}^{n_c}c(\ell)\left(_{n+(1/2)}H_{i+\ell,j+(1/2)}^{y,\psi\psi} - {_{n+(1/2)}}H_{i-\ell,j+(1/2)}^{y,\psi\psi}\right) - \frac{1}{\Delta y}\sum_{\ell=1}^{n_d}d(\ell)\left(_{n+(1/2)}H_{i,j+\ell+(1/2)}^{x,\phi\phi} - {_{n+(1/2)}}H_{i,j-\ell+(1/2)}^{x,\phi\phi}\right) \quad (21)$$

$$\frac{\epsilon}{\Delta t}\left(_{n+1}E_{i+(1/2),j}^{z,\psi\phi} - {_n}E_{i+(1/2),j}^{z,\psi\phi}\right)$$

$$=\frac{1}{\Delta x}\sum_{\ell=1}^{n_b}b(\ell)\left(_{n+(1/2)}H_{i+\ell,j}^{y,\psi\phi} - {_{n+(1/2)}}H_{i-\ell+1,j}^{y,\psi\phi}\right) - \frac{1}{\Delta y}\sum_{\ell=1}^{n_a}a(\ell)\left(_{n+(1/2)}H_{i+(1/2),j+\ell-(1/2)}^{x,\psi\phi} - {_{n+(1/2)}}H_{i+(1/2),j-\ell+(1/2)}^{x,\psi\phi}\right)$$

$$+\frac{1}{\Delta x}\sum_{\ell=1}^{n_d}d(\ell)\left(_{n+(1/2)}H_{i+\ell+(1/2),j}^{y,\phi\phi} - {_{n+(1/2)}}H_{i-\ell+(1/2),j}^{y,\phi\phi}\right) - \frac{1}{\Delta y}\sum_{\ell=1}^{n_c}c(\ell)\left(_{n+(1/2)}H_{i+(1/2),j+\ell}^{x,\psi\psi} - {_{n+(1/2)}}H_{i+(1/2),j-\ell}^{x,\psi\psi}\right) \quad (22)$$

$$\frac{\epsilon}{\Delta t}\left(_{n+1}E_{i+(1/2),j+(1/2)}^{z,\psi\psi} - {_n}E_{i+(1/2),j+(1/2)}^{z,\psi\psi}\right)$$

$$=\sum_{\ell=1}^{n_b}b(\ell)\left[\frac{1}{\Delta x}\left(_{n+(1/2)}H_{i+\ell-(1/2),j+(1/2)}^{y,\psi\psi} - {_{n+(1/2)}}H_{i-\ell+(1/2),j+(1/2)}^{y,\psi\psi}\right) - \frac{1}{\Delta y}\left(_{n+(1/2)}H_{i+(1/2),j+\ell}^{x,\psi\psi} - {_{n+(1/2)}}H_{i+(1/2),j-\ell+1}^{x,\psi\psi}\right)\right]$$

$$+\sum_{\ell=1}^{n_d}d(\ell)\left[\frac{1}{\Delta x}\left(_{n+(1/2)}H_{i+\ell+(1/2),j+(1/2)}^{y,\phi\psi} - {_{n+(1/2)}}H_{i-\ell+(1/2),j+(1/2)}^{y,\phi\psi}\right)\right.$$

$$\left. -\frac{1}{\Delta y}\left(_{n+(1/2)}H_{i+(1/2),j+\ell+(1/2)}^{x,\psi\phi} - {_{n+(1/2)}}H_{i+(1/2),j-\ell+(1/2)}^{x,\psi\phi}\right)\right]. \quad (23)$$

Meanwhile, the 2-D W-MRTD magnetic field basis function coefficients are updated using (24)–(31) that follow:

$$\frac{\mu}{\Delta t}\left(_{n+(1/2)}H_{i,j+(1/2)}^{x,\phi\phi} - {_{n-(1/2)}}H_{i,j+(1/2)}^{x,\phi\phi}\right)$$

$$=-\frac{1}{\Delta y}\sum_{\ell=1}^{n_a}a(\ell)\left(_{n}E_{i,j+\ell}^{z,\phi\phi} - {_n}E_{i,j-\ell+1}^{z,\phi\phi}\right)$$

$$-\frac{1}{\Delta y}\sum_{\ell=1}^{n_c}c(\ell)\left(_{n}E_{i,j+\ell+(1/2)}^{z,\phi\psi} - {_n}E_{i,j-\ell+(1/2)}^{z,\phi\psi}\right) \quad (24)$$

$$\frac{\mu}{\Delta t}\left(_{n+(1/2)}H_{i,j}^{x,\phi\psi} - {_{n-(1/2)}}H_{i,j}^{x,\phi\psi}\right)$$

$$=-\frac{1}{\Delta y}\sum_{\ell=1}^{n_b}b(\ell)\left(_{n}E_{i,j+\ell-(1/2)}^{z,\phi\psi} - {_n}E_{i,j-\ell+(1/2)}^{z,\phi\psi}\right)$$

$$-\frac{1}{\Delta y}\sum_{\ell=1}^{n_d}d(\ell)\left(_{n}E_{i,j+\ell}^{z,\phi\phi} - {_n}E_{i,j-\ell}^{z,\phi\phi}\right) \quad (25)$$

$$\frac{\mu}{\Delta t}\left(_{n+(1/2)}H_{i+(1/2),j+(1/2)}^{x,\psi\phi} - {_{n-(1/2)}}H_{i+(1/2),j+(1/2)}^{x,\psi\phi}\right)$$

$$=-\frac{1}{\Delta y}\sum_{\ell=1}^{n_a}a(\ell)\left(_{n}E_{i+(1/2),j+\ell}^{z,\psi\phi} - {_n}E_{i+(1/2),j-\ell+1}^{z,\psi\phi}\right)$$

$$-\frac{1}{\Delta y}\sum_{\ell=1}^{n_c}c(\ell)\left(_{n}E_{i+(1/2),j+\ell+(1/2)}^{z,\psi\psi} - {_n}E_{i+(1/2),j-\ell+(1/2)}^{z,\psi\psi}\right) \quad (26)$$

$$\frac{\mu}{\Delta t}\left(_{n+(1/2)}H_{i+(1/2),j}^{x,\psi\psi} - {_{n-(1/2)}}H_{i+(1/2),j}^{x,\psi\psi}\right)$$

$$=-\frac{1}{\Delta y}\sum_{\ell=1}^{n_b}b(\ell)\left(_{n}E_{i+(1/2),j+\ell-(1/2)}^{z,\psi\psi} - {_n}E_{i+(1/2),j-\ell+(1/2)}^{z,\psi\psi}\right)$$

$$-\frac{1}{\Delta y}\sum_{\ell=1}^{n_d}d(\ell)\left(_{n}E_{i+(1/2),j+\ell}^{z,\psi\phi} - {_n}E_{i+(1/2),j-\ell}^{z,\psi\phi}\right) \quad (27)$$

$$\frac{\mu}{\Delta t}\left(_{n+(1/2)}H_{i+(1/2),j}^{y,\phi\phi} - {_{n-(1/2)}}H_{i+(1/2),j}^{y,\phi\phi}\right)$$

$$=\frac{1}{\Delta x}\sum_{\ell=1}^{n_a}a(\ell)\left(_{n}E_{i+\ell,j}^{z,\phi\phi} - {_n}E_{i-\ell+1,j}^{z,\phi\phi}\right)$$

$$+\frac{1}{\Delta x}\sum_{\ell=1}^{n_c}c(\ell)\left(_{n}E_{i+\ell+(1/2),j}^{z,\psi\phi} - {_n}E_{i-\ell+(1/2),j}^{z,\psi\phi}\right) \quad (28)$$

$$\frac{\mu}{\Delta t}\left(_{n+(1/2)}H_{i+(1/2),j+(1/2)}^{y,\phi\psi} - {_{n-(1/2)}}H_{i+(1/2),j+(1/2)}^{y,\phi\psi}\right)$$

$$=\frac{1}{\Delta x}\sum_{\ell=1}^{n_a}a(\ell)\left(_{n}E_{i+\ell,j+(1/2)}^{z,\phi\psi} - {_n}E_{i-\ell+1,j+(1/2)}^{z,\phi\psi}\right)$$

$$+\frac{1}{\Delta x}\sum_{\ell=1}^{n_c}c(\ell)\left(_{n}E_{i+\ell+(1/2),j+(1/2)}^{z,\psi\psi} - {_n}E_{i-\ell+(1/2),j+(1/2)}^{z,\psi\psi}\right) \quad (29)$$

$$\frac{\mu}{\Delta t}\left(_{n+(1/2)}H_{i,j}^{y,\psi\phi} - {_{n-(1/2)}}H_{i,j}^{y,\psi\phi}\right)$$

$$=\frac{1}{\Delta x}\sum_{\ell=1}^{n_b}b(\ell)\left(_{n}E_{i+\ell-(1/2),j}^{z,\psi\phi} - {_n}E_{i-\ell+(1/2),j}^{z,\psi\phi}\right)$$

$$+\frac{1}{\Delta x}\sum_{\ell=1}^{n_d}d(\ell)\left(_{n}E_{i+\ell,j}^{z,\phi\phi} - {_n}E_{i-\ell,j}^{z,\phi\phi}\right) \quad (30)$$

$$\frac{\mu}{\Delta t}\left(_{n+(1/2)}H_{i,j+(1/2)}^{y,\psi\psi} - {_{n-(1/2)}}H_{i,j+(1/2)}^{y,\psi\psi}\right)$$

$$=\frac{1}{\Delta x}\sum_{\ell=1}^{n_b}b(\ell)\left(_{n}E_{i+\ell-(1/2),j+(1/2)}^{z,\psi\psi} - {_n}E_{i-\ell+(1/2),j+(1/2)}^{z,\psi\psi}\right)$$

$$+\frac{1}{\Delta x}\sum_{\ell=1}^{n_d}d(\ell)\left(_{n}E_{i+\ell,j+(1/2)}^{z,\phi\psi} - {_n}E_{i-\ell,j+(1/2)}^{z,\phi\psi}\right). \quad (31)$$

REFERENCES

[1] K. L. Shlager and J. B. Schneider, "Comparison of the dispersion properties of several low-dispersion finite-difference time-domain algorithms," *IEEE Trans. Antennas Propagat.*, vol. 51, pp. 642–653, Mar. 2003.
[2] J. Fang, "Time domain finite difference computation for Maxwell's equations," Ph.D. dissertation, Univ. of California at Berkeley, Berkeley, CA, 1989.
[3] C. W. Manry, S. L. Broschat, and J. B. Schneider, "Higher-order FDTD methods for large problems," *Appl. Comput. Electromagn. Soc. J.*, vol. 10, no. 2, pp. 17–29, 1995.
[4] J. Zhang and Z. Chen, "Low-dispersive super high-order FDTD schemes," in *IEEE Antennas Propagat. Soc. Int. Symp.*, vol. 3, Salt Lake City, UT, July 2000, pp. 1510–1513.
[5] M. Krumpholz and L. P. B. Katehi, "MRTD: New time-domain schemes based on multiresolution analysis," *IEEE Trans. Microwave Theory Tech.*, vol. 44, pp. 555–571, Apr. 1996.
[6] T. Dogaru and L. Carin, "Multiresolution time-domain using CDF biorthogonal wavelets," *IEEE Trans. Microwave Theory Tech.*, vol. 49, pp. 902–912, May 2001.
[7] X. Wei, E. Li, and C. Liang, "A new MRTD scheme based on Coifman scaling functions for the solution of scattering problems," *IEEE Microwave Wireless Comp. Lett.*, vol. 12, pp. 392–394, Oct. 2002.
[8] *Personal Communication from T. Dogaru*
[9] S. Wolfram, *The Mathematica Book*, 4 ed. Cambridge, U.K.: Cambridge Univ. Press, 1999.

Kurt L. Shlager (S'81–M'88–SM'02) received the B.S. degree in electrical engineering from Southeastern Massachusetts University (now UMass at Dartmouth), North Dartmouth, the M.S. degree in electrical engineering from Tufts University, Medford, MA, and the Ph.D. degree in electrical engineering from the Georgia Institute of Technology, Atlanta, in 1985, 1987, and 1995, respectively.

He has been with GTE Government Systems, Westborough, MA; TRW Space and Electronics Group, Redondo Beach, CA; Space Systems Loral, Palo Alto, CA; and Lockheed-Martin Space Systems Company, Sunnyvale, CA, where he is presently a Staff Engineer. His research interests include the finite-difference time-domain method, electromagnetic scattering, and antenna analysis and design. He coauthored the chapter "A Survey of the Finite-Difference Time-Domain Literature" in *Advances in Computational Electrodynamics: The Finite-Difference Time-Domain Method* (Reading, MA: Artech House, 1998). He has published approximately 25 refereed journal and conference papers.

John B. Schneider received the B.S. degree from Tulane University of Louisiana, New Orleans, and the M.S. and Ph.D. degrees from the University of Washington, Seattle, all in electrical engineering.

He is presently an Associate Professor in the School of Electrical Engineering and Computer Science, Washington State University, Pullman. His research interests include the use of computational methods to analyze acoustic, elastic, and electromagnetic wave propagation.